

## Chapter 3

### Visible Light Photoactivity of Nitrogen-Doped TiO<sub>2</sub>

## Abstract

Titanium dioxide was doped with nitrogen atoms via high temperature treatment with ammonia, toward the goal of developing a catalyst capable of using visible light to degrade organic substrates. Catalyst efficiency was tested by monitoring formate degradation to CO<sub>2</sub> and H<sub>2</sub>O under visible light using ion chromatography. However, reduced photocatalytic activity in the UV region, as well as a strong synthesis temperature dependence on catalytic efficiency, was observed. The N-doped TiO<sub>2</sub> surface was probed with diffuse infrared Fourier transform spectroscopy (DRIFTS), leading us to conclude that Ti–N triple bond defect sites control visible light activity and lead to an apparent reduction in overall crystallinity.

## Introduction

TiO<sub>2</sub> is of great interest in the field of heterogeneous photocatalysis. TiO<sub>2</sub> has the advantage of being cheap, nontoxic, and stable, all of which make it attractive for remediation of environmental organic pollutants.<sup>1</sup> However, its wide bandgap (3.2 eV) means that it can only utilize ~5% of the solar spectrum, all in the UV region. If this threshold energy could be reduced, visible light could then be used, opening up a much larger portion of the solar spectrum for potential photocatalytic work.

A large number of approaches have been taken to reduce the bandgap energy of TiO<sub>2</sub>, such as doping with transition metal cations,<sup>2-5</sup> creating oxygen vacancies,<sup>6</sup> or, most recently, doping with anions such as C,<sup>7-9</sup> S,<sup>10,11</sup> and N.<sup>12-17</sup> Progress to date on nitrogen-doped TiO<sub>2</sub> (henceforth referred to as N-TiO<sub>2</sub>) was covered in a recent review paper.<sup>18</sup> The first report of N-TiO<sub>2</sub> was by Asahi et al.<sup>12</sup> in 2001, in which they bleached methylene blue (MB). It was originally believed that mixing of nitrogen 2p states with lattice oxygen 2p states led to an overall reduction in the bandgap energy. However, more recent studies<sup>14,19,20</sup> have shown both theoretically and experimentally that either substitutionally or interstitially bound nitrogen species result in localized N 2p states above the valence band.

Our goal was to optimize the synthesis conditions to create the most catalytically efficient N-TiO<sub>2</sub>, and to measure its potential to degrade a typical aqueous organic contaminant, such as formate, using visible light. We had previously achieved partial success in the visible light photocatalysis of formate oxidation, however reproducibility issues led us to publish that formate could not be oxidized by N-TiO<sub>2</sub>.<sup>16</sup> On the other

hand, depending of the exact conditions of preparation a variety of N-TiO<sub>2</sub> catalysts have been shown to be photoactive with visible light.

## Experimental

Anatase TiO<sub>2</sub> (99.9%, Aldrich), TiO<sub>2</sub> (Degussa P25; 25% rutile, 75% anatase), TiN (Aldrich), and sodium formate (Aldrich) were used as received. Oxygen gas (99.9%) was passed through a water trap before use in the FTIR experiments. N-TiO<sub>2</sub> catalysts were made by high-temperature nitridation.<sup>12,21</sup> The TiO<sub>2</sub> powders were first treated between 500 and 600 °C under NH<sub>3</sub>/Ar (80:20) gas flow at 1 atm for 3 hours, and then subsequently treated under air for 1 hour.

UV-vis diffuse reflectance spectra were recorded on a Shimadzu UV-2101PC with an integrating sphere attachment (Shimadzu ISR-260), using Ba<sub>2</sub>SO<sub>4</sub> powder as an internal reference. XPS experiments were performed in an M-probe surface spectrometer (VG Instruments) using monochromatic Al K $\alpha$  X-rays (1486.6 eV). Formate degradation was analyzed by using a Dionex DX500 ion chromatograph (Dionex IonPac AS11 column) equipped with a conductivity detector.

DRIFT spectra were acquired using a Bio-Rad FTS-45 spectrometer with a liquid N<sub>2</sub>-cooled MCT detector. Spectra were collected at 8 cm<sup>-1</sup> resolution using a Spectra-Tech Collector diffuse-reflectance accessory. The solid samples were held in the sample cup of a Spectra-Tech high temperature environmental chamber (HTEC) that could be resistively heated to 1000 K ( $\pm 1$  K), and the chamber evacuated to 10  $\mu$ Torr. A gas manifold connected to the sample chamber allowed for O<sub>2</sub> gas to be introduced and removed as needed. UV radiation from a 1 kW Oriel Xe lamp was focused into the HTEC chamber through a moveable mirror and lens system that allowed for photolysis experiments to be conducted without breaking system purge.

Photolysis experiments were performed by using the collimated output of a high-pressure Hg-Xe arc lamp as a light source. The light beam was passed through an IR filter, two focusing lenses, a 320 nm cutoff filter, and a 400 nm cutoff filter before reaching the reactor. The reactor (sample volume = 26 mL) was surrounded by a water jacket on all sides except for the side receiving the light beam, which instead had a quartz window. The surrounding water jacket was cooled by a recirculating water bath and kept at 12 °C. The reactor was constantly aerated by compressed air to keep a steady level of O<sub>2</sub>. Figure 3.1 shows the experimental setup.

For the photodegradation experiments, the formate ion concentration was 15 mg/L (0.33 mM), the catalyst loading was 0.5 g/L, the solvent was water, the reaction solution was at pH 7, and the lamp power was 1000 W. Aliquots of the reaction mixture were syringed out in 1 mL volumes through a plastic syringe at various time intervals, filtered through a 0.2 μm filter to remove the catalyst, and analyzed by ion chromatography (IC). The IC instrument required less than 100 μL solution for each measurement, thus several data points were collected at each time point to ensure accuracy.

## Results and Discussion

Table 3.1 summarizes the different nitrogen-containing materials that were synthesized. For all but one sample, the starting material was TiO<sub>2</sub> (either P25 or anatase), which was then placed into a tube furnace and heated under a mixed Ar/NH<sub>3</sub> atmosphere at temperatures ranging from 500 to 600 °C for 3 hours. A portion of the sample was then reheated for 1 hour under air. The anatase powders became yellow after the initial NH<sub>3</sub> treatment, whereas the P25 powders became various shades of blue. Upon air reheating, all sample powders became either a pale yellow (anatase samples) or white (P25 samples). Alternatively, TiN was used as a starting material, which was then placed into the furnace and heated under air flow at 550 °C, leading to a light-brown powder.

Prior to the reheat step in air, catalytic activity for formate degradation was quite low. Furthermore, the anatase samples were consistently better catalysts than the P25 samples and the oxidized TiN sample, so after some initial degradation experiments, only anatase samples were used. Theoretical studies have shed some insight into why anatase makes the better starting material than P25, namely that nitrogen-doping in rutile TiO<sub>2</sub> contracts the valence band state and actually increases the effective bandgap.<sup>14</sup> Figure 3.2 (top) shows the photocatalytic activity of the reheated anatase N-TiO<sub>2</sub> materials (samples 8, 9, and 10) as well as the parent anatase material for degrading formate under UV irradiation (>320 nm). Under UV light, anatase is the best catalyst, completely oxidizing formate in 1 hour under the experimental conditions. The material created at 500 °C (sample 9) show the next best formate degradation, taking 90 minutes to completely degrade formate. The materials created at 550 °C (sample 10) and 600 °C (sample 8) showed a marked dropoff in the ability to degrade formate under UV light.

Figure 3.2 (bottom) shows the same samples, but under visible irradiation ( $>400$  nm). Under visible light, sample 10 showed the best activity, followed by sample 9. Sample 8 showed little activity, nor did anatase powder, as expected.

Figure 3.3 shows the UV-vis diffuse reflectance powder spectra for the best performing anatase catalyst (sample 10), its starting material (sample 3), oxidized TiN, and anatase powder. All 3 modified-TiO<sub>2</sub> powders have an absorption edge that stretches into the visible, although the catalyst with the least prominent absorption edge (sample 10) is actually the best catalyst. It is thus unwise to extrapolate photocatalytic activity based on absorption spectra, even though the literature on N-TiO<sub>2</sub> often prominently displays such spectra as evidence of improved visible light photoactivity.

Figure 3.4 shows the XPS spectra in the N region for TiN, as well as oxidized TiN and sample 10. For the latter 2 samples, Ar<sup>+</sup> sputtering was used (60 s, 4 keV). In contrast to the published literature, no nitrogen XPS peak was observed, indicating either low ( $< 0.5\%$ ) nitrogen content, or subsurface nitrogen that was either too deep to be seen by sputtering or removed by the sputtering process.

Figure 3.5 shows a series of DRIFT spectra monitoring the oxidation process of titanium nitride. Note that it was not possible to collect DRIFT spectra of the pure black TiN starting material, even after diluting with KBr powder, due to broad IR absorption. After the initial 3-hour heating period in air at 550 °C (figure 3.5a), there is a strong single peak at 3271 cm<sup>-1</sup>, which is assigned to the primary amine Ti-NH<sub>2</sub>. There are also bridging hydroxyl groups seen at 3414 cm<sup>-1</sup> and Ti-OH at 3645 cm<sup>-1</sup>, which are consistent with earlier work.<sup>22</sup> Further oxidation (figure 3.5b and 3.5c), this time under dry oxygen atmosphere, reduces the intensity of all 3 species. The loss of the amine

functionality is a result of replacing Ti–N bonds with Ti–O bonds, whereas surface dehydration accounts for the loss of the O–H species. A further oxidation step (figure 3.5d) using wet oxygen leads to the recovery of the bridging hydroxyl and Ti–OH peaks, which is consistent with surface rehydration, most likely into oxygen vacancy sites created by the heating process.<sup>23</sup>

Figure 3.6 shows the DRIFT spectra of the intermediate catalysts (samples 2, 3 and 6), while figure 3.7 shows the DRIFT spectra of the final catalysts (samples 8, 9, and 10). The most prominent feature in the intermediate catalysts, besides the Ti–OH group at  $3672\text{ cm}^{-1}$ , is the appearance of a sharp peak at  $3156\text{ cm}^{-1}$ . This peak is neither in the starting material, anatase, or the reheated product, as shown in figure 3.8. Thus, it is likely a nitrogen species such as a bridged N–H group in the form of Ti–N(H)–Ti. The most notable feature in the final catalysts is the presence of peak or peaks in the IR region associated with triple bonds. The lowest temperature catalyst, sample 9, has no features. Sample 10, which was synthesized at the intermediate temperature ( $550\text{ }^{\circ}\text{C}$ ), has one sharp peak at  $2145\text{ cm}^{-1}$ . The high temperature catalyst, sample 9, has 2 additional peaks at  $2164\text{ cm}^{-1}$  and  $2195\text{ cm}^{-1}$ . Metal-nitrogen triple bonds are not unknown,<sup>24</sup> and these species are tentatively assigned to a Ti–N triple bond. Several groups have examined Ti–N bonded species by FTIR, and have found species with strong adsorptions in this spectral region. The Ti–NCO species has been thoroughly examined,<sup>25,26</sup> and it was found that the main absorption frequency, assigned to asymmetric  $\nu(\text{NCO})$ , falls in the range of  $2170\text{--}2320\text{ cm}^{-1}$ . Rusu and Yates looked at the adsorption of  $\text{N}_2\text{O}$  on  $\text{TiO}_2$ ,<sup>27</sup> and reported Ti–ONN and Ti–NNO peaks in this region as well (note however that their experiments were conducted at  $157\text{ K}$ , as adsorbed  $\text{N}_2\text{O}$  is completely desorbed at room

temperature). However, the literature results are not sufficient to explain both the location and number of peaks found in this work. Thus, the multiple peaks in the high temperature sample likely indicate multiple chemical environments for the Ti–N triple bonds, a result of catalyst inhomogeneity caused by loss of crystallinity. This helps explain the reduced catalytic activity of the high temperature sample compared to the intermediate temperature sample. And the much higher UV photocatalytic activity of the lower temperature catalyst (sample 9) compared to the higher temperature catalysts is likely from the absence of these Ti–N triple bond sites, and thus higher crystallinity.

The Ti–N triple bond species was further probed by treating the catalyst with UV light, both under oxygen atmosphere and *in vacuo*. UV treatment under oxygen had no effect on the  $2145\text{ cm}^{-1}$  peak intensity. However, UV treatment *in vacuo* led to an increase in peak intensity, as seen in figure 3.9. There is also loss of surface Ti–OH groups, as well as a loss of a broad absorption band found between  $3000$  and  $3500\text{ cm}^{-1}$  that is most likely surface water. This spectral region is also the region in which N–H bonds appear, so the loss of N–H bonds is a possibility as well. Literature evidence supports an interstitially bound N–H species as the active dopant.<sup>28</sup> The increase in Ti–N triple bonds could be caused by a rearrangement of interstitially bound N–H groups into a higher-energy triple-bond state. UV treatment *in vacuo* creates oxygen vacancies, and if these vacancies are created next to a Ti atom interstitially bound N–H, it is possible that there is surface rearrangement, with the N atom filling the oxygen-defect site, and increasing its bond order with respect to its closest Ti atom. The lack of increased signal strength upon treatment under oxygen lends support to the idea that oxygen-defect sites play a role in the formation of the Ti–N triple-bond species, as oxygen defects are not

generated during UV treatment under oxygen atmosphere. Alternatively, the UV treatment, which removes less-weakly-bound surface species, could cause an enhancement of the Ti–N triple bond signal due to less interference from the removed surface layer of water.

In an alternate reheating process, sample 3 was heated to 200 °C and exposed to UV light, while under oxygen, in the HTEC DRIFTS chamber, as shown in figure 3.10. Loss of intensity at 3156  $\text{cm}^{-1}$  (Ti–OH) is observed, however there is no peak at 2145  $\text{cm}^{-1}$ , evidence that this species is likely only produced at high temperatures.

## Conclusions

N-TiO<sub>2</sub> created by high temperature ammonia treatment of anatase TiO<sub>2</sub> powder has shown to be an active catalyst in degradation of formate under visible light, extending the useable wavelength region of the starting material. However the catalytic efficiency of the doped catalyst under UV light is less than the starting material. FTIR evidence suggest the visible light active catalysts have defect sites in the form of Ti–N triple bonds, and that the increase of these sites leads to loss of crystallinity that accounts for the reduced UV photocatalytic activity. Thus, the optimal synthesis temperature of 550 °C can be seen as a balance point between catalyst crystallinity and the presence of defect sites that can absorb visible light photons.

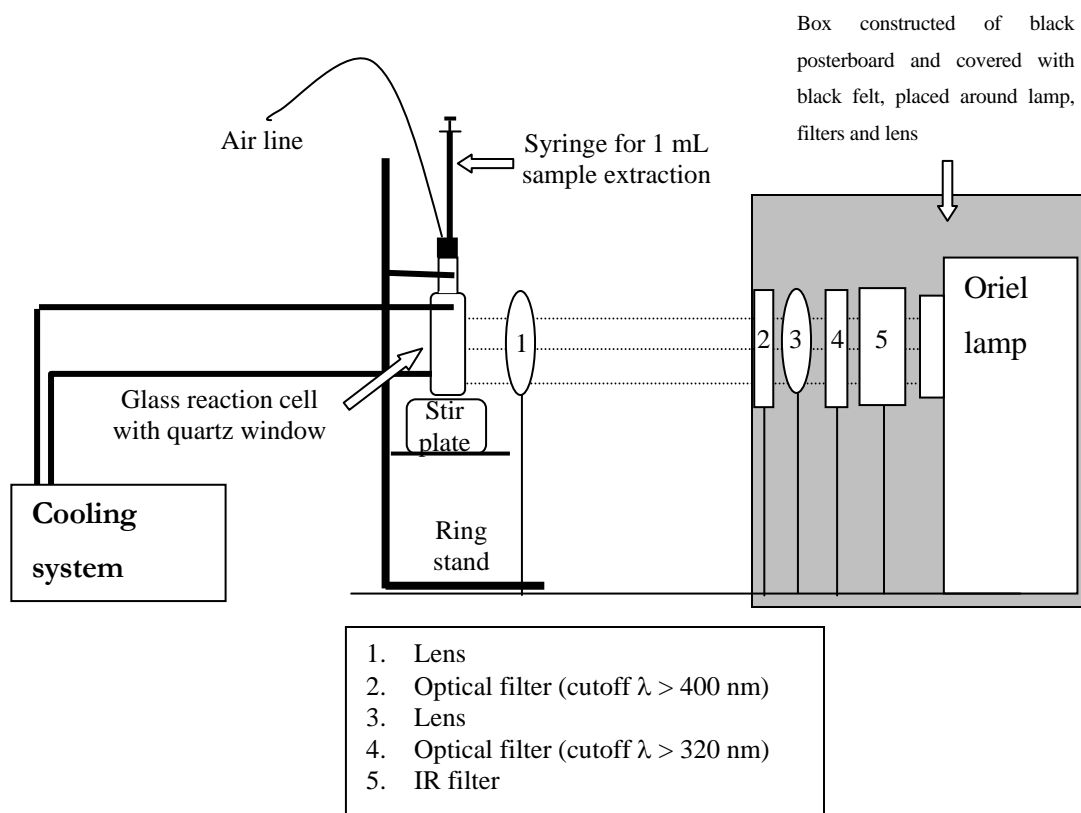


**Figure 3.1.** Experimental setup for formate degradation experiments.

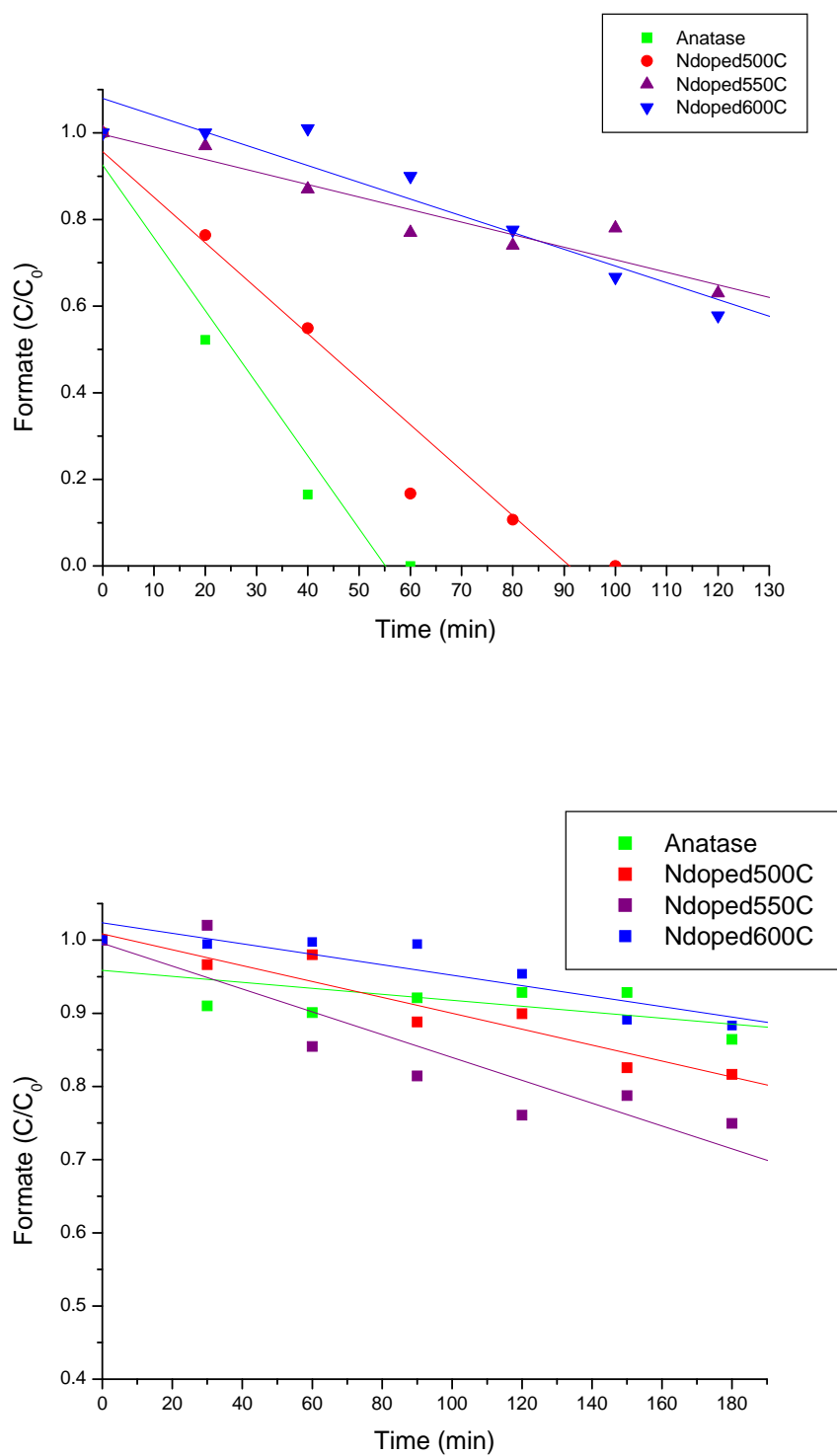


**Figure 3.2.** Formate degradation results under UV light (top) and visible light (bottom).

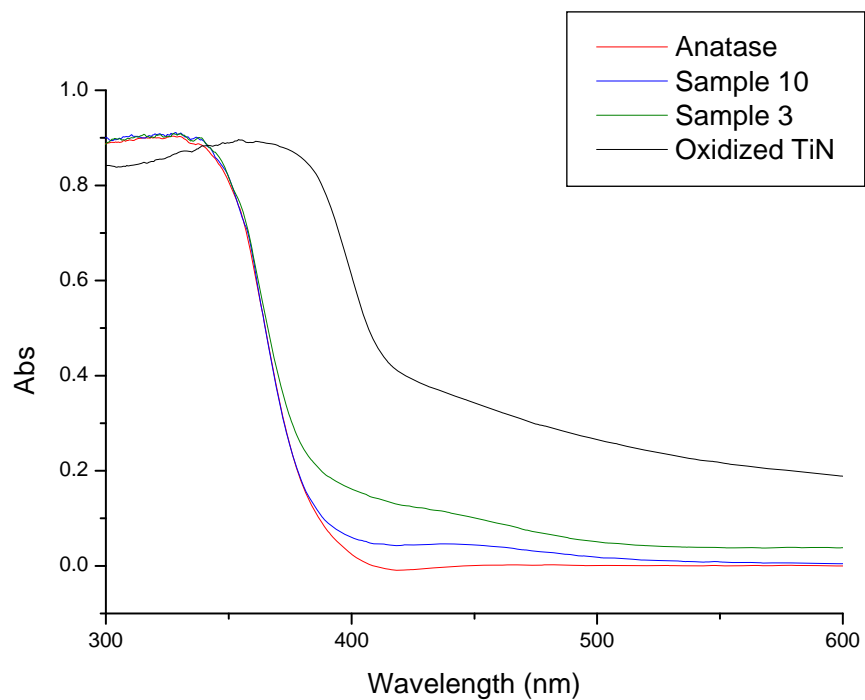


**Figure 3.3.** UV-vis diffuse reflectance powder spectra for the best anatase catalyst (sample 10), its starting material (sample 3), oxidized TiN, and anatase TiO<sub>2</sub>.

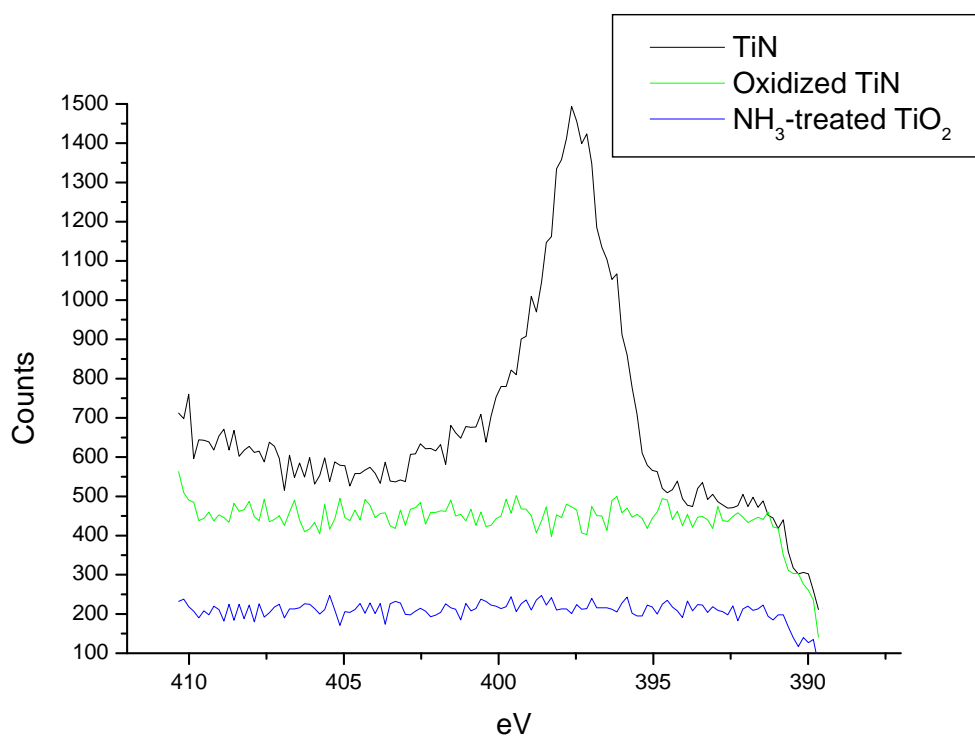


**Figure 3.4.** XPS spectra of N region for TiN, oxidized TiN, and NH<sub>3</sub> treated anatase powder (sample 10).

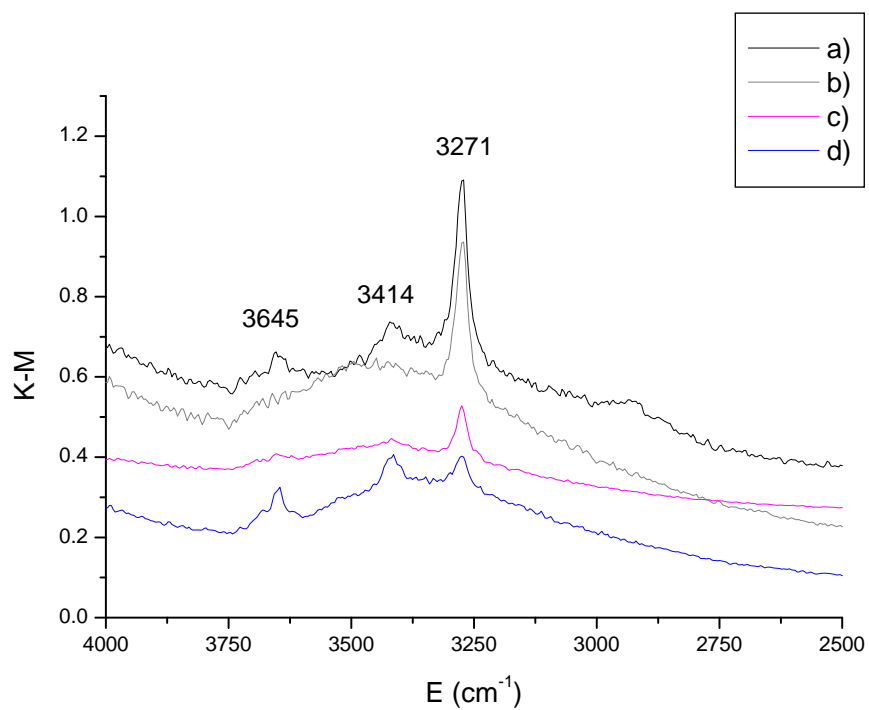


**Figure 3.5.** a) TiN after 3 hours of oxidation in air b) plus an additional 3 hours oxidation under dry oxygen atmosphere c) plus an additional 12 hours oxidation under dry oxygen atmosphere d) plus an additional 1 hour oxidation under wet oxygen atmosphere.

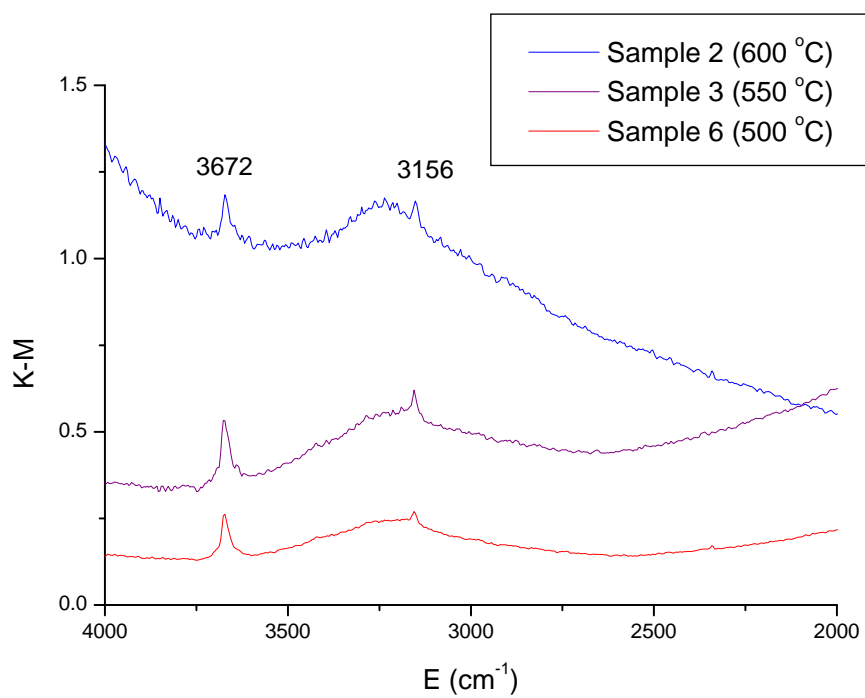


**Figure 3.6.** DRIFT spectra of the three intermediate catalysts (samples 2, 3, and 6).

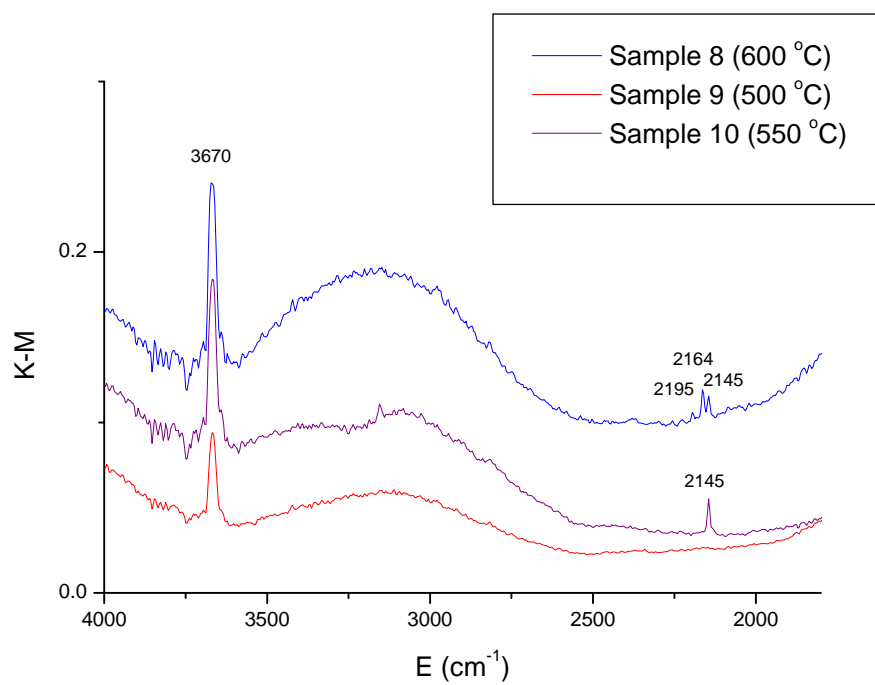


**Figure 3.7.** DRIFT spectra of the reheated, final catalysts (samples 8, 9 and 10).

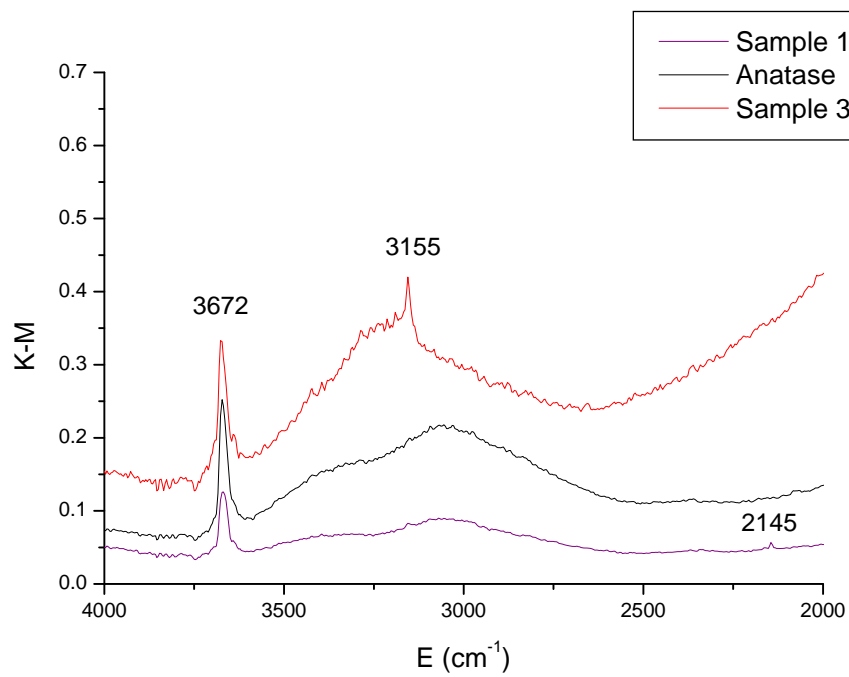


**Figure 3.8.** DRIFT spectra of the starting material (anatase), the intermediate catalyst (sample 3), and the final catalyst (sample 10).

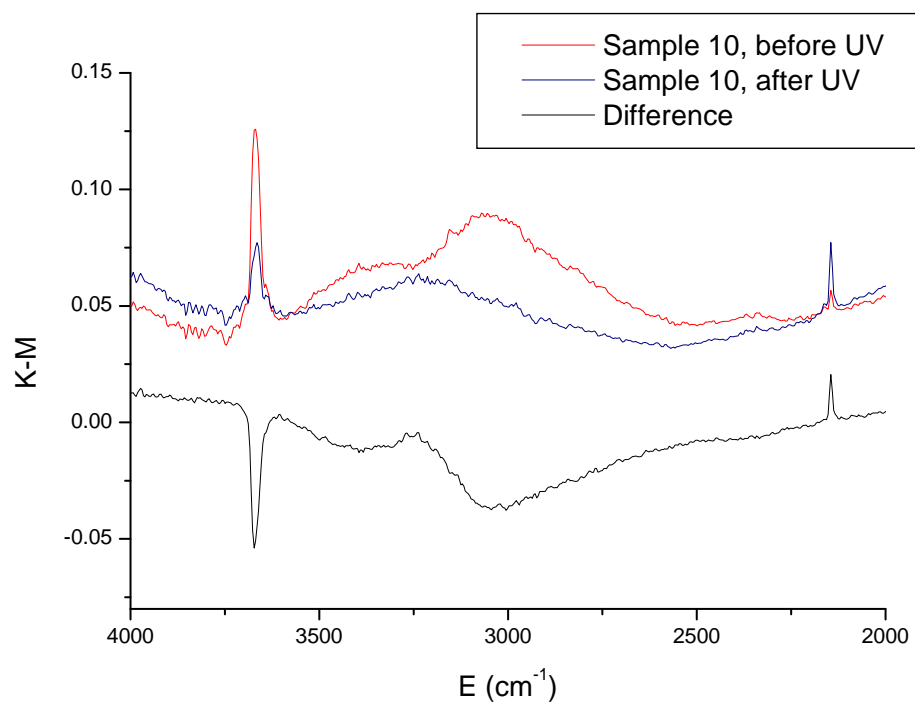


**Figure 3.9.** DRIFT spectra of the sample 10, before and after UV treatment *in vacuo*.

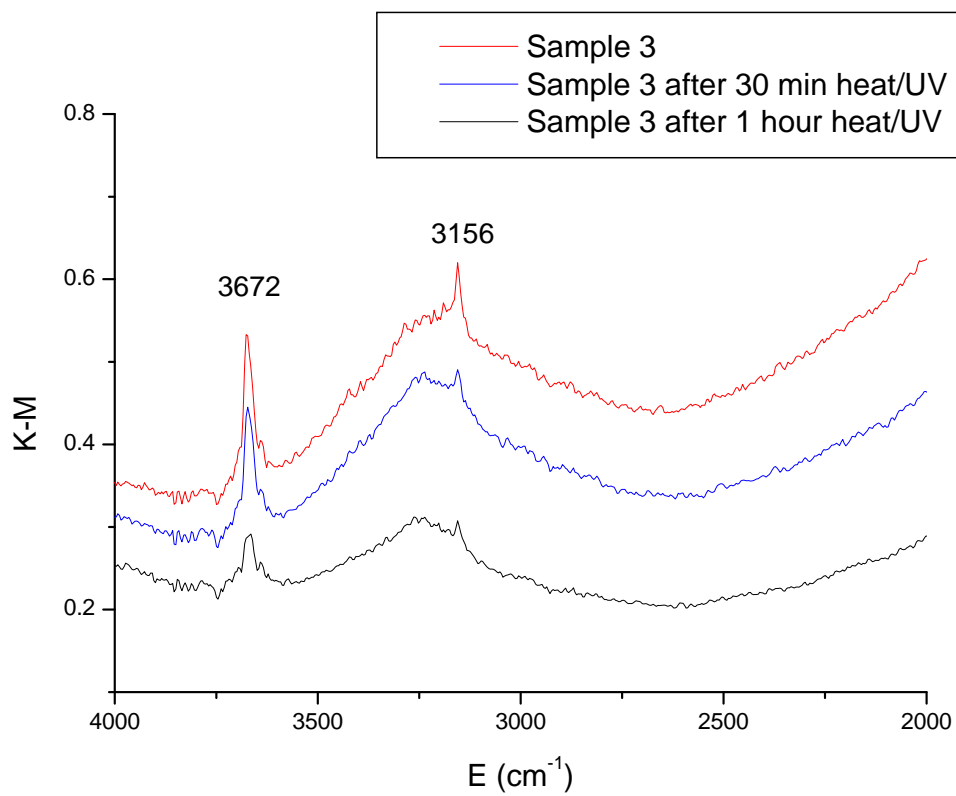


**Figure 3.10.** DRIFT spectra of the sample 3 undergoing heat (200 °C) and UV treatment under oxygen atmosphere.

Sample number	Parent material	Preparation procedure
<b>1</b>	P-25	Heating in argon-ammonia atmosphere T = 600 °C; t = 3 h; Ar: 6 dm <sup>3</sup> /h NH <sub>3</sub> : 12 dm <sup>3</sup> /h
<b>2</b>	Anatase	
<b>3</b>	Anatase	Heating in argon-ammonia atmosphere T = 550 °C; t = 3 h; Ar: 3 dm <sup>3</sup> /h NH <sub>3</sub> : 12 dm <sup>3</sup> /h
<b>4</b>	P-25	
<b>5</b>	P-25	Heating in argon-ammonia atmosphere T = 500 °C; t = 3 h; Ar: 3 dm <sup>3</sup> /h NH <sub>3</sub> : 12 dm <sup>3</sup> /h
<b>6</b>	Anatase	
<b>7</b>	TiN	Oxidation in air, t = 3 h;
<b>8</b>	Sample 2	Reheating in air: T = 550 °C; t = 1 h;
<b>9</b>	Sample 6	
<b>10</b>	Sample 3	

**Table 3.1.** Synthesis conditions for preparation of N-TiO<sub>2</sub> powders

## References

- (1) Hoffmann, M. R.; Martin, S. T.; Choi, W. Y.; Bahnemann, D. W. *Chem. Rev.* **1995**, *95*, 69.
- (2) Anpo, M.; Ichihashi, Y.; Takeuchi, M.; Yamashita, H. *Res. Chem. Intermed.* **1998**, *24*, 143.
- (3) Choi, W. Y.; Termin, A.; Hoffmann, M. R. *Angew. Chem. Int. Ed.* **1994**, *33*, 1091.
- (4) Choi, W. Y.; Termin, A.; Hoffmann, M. R. *J. Phys. Chem.* **1994**, *98*, 13669.
- (5) Li, X. Z.; Li, F. B. *Environ. Sci. Technol.* **2001**, *35*, 2381.
- (6) Nakamura, I.; Negishi, N.; Kutsuna, S.; Ihara, T.; Sugihara, S.; Takeuchi, E. *J. Mol. Catal. A: Chem.* **2000**, *161*, 205.
- (7) Sakthivel, S.; Kisch, H. *Angew. Chem. Int. Ed.* **2003**, *42*, 4908.
- (8) Khan, S. U. M.; Al-Shahry, M.; Ingler, W. B. *Science* **2002**, *297*, 2243.
- (9) Nakano, Y.; Morikawa, T.; Ohwaki, T.; Taga, Y. *Appl. Phys. Lett.* **2005**, *87*.
- (10) Umebayashi, T.; Yamaki, T.; Itoh, H.; Asai, K. *Appl. Phys. Lett.* **2002**, *81*, 454.
- (11) Umebayashi, T.; Yamaki, T.; Tanaka, S.; Asai, K. *Chem. Lett.* **2003**, *32*, 330.
- (12) Asahi, R.; Morikawa, T.; Ohwaki, T.; Aoki, K.; Taga, Y. *Science* **2001**, *293*, 269.
- (13) Chen, X. B.; Burda, C. *J. Phys. Chem. B* **2004**, *108*, 15446.
- (14) Di Valentin, C.; Pacchioni, G.; Selloni, A. *Phys. Rev. B* **2004**, *70*.
- (15) Lee, J. Y.; Park, J.; Cho, J. H. *Appl. Phys. Lett.* **2005**, *87*.

- (16) Mrowetz, M.; Balcerski, W.; Colussi, A. J.; Hoffman, M. R. *J. Phys. Chem. B* **2004**, *108*, 17269.
- (17) Sato, S.; Nakamura, R.; Abe, S. *Appl. Catal., A* **2005**, *284*, 131.
- (18) Thompson, T. L.; Yates, J. T. *Chem. Rev.* **2006**, *106*, 4428.
- (19) Batzill, M.; Morales, E. H.; Diebold, U. *Phys. Rev. Lett.* **2006**, *96*, 026103.
- (20) Di Valentin, C.; Pacchioni, G.; Selloni, A.; Livraghi, S.; Giamello, E. *J. Phys. Chem. B* **2005**, *109*, 11414.
- (21) Irie, H.; Watanabe, Y.; Hashimoto, K. *J. Phys. Chem. B* **2003**, *107*, 5483.
- (22) Szczepankiewicz, S. H.; Colussi, A. J.; Hoffmann, M. R. *J. Phys. Chem. B* **2000**, *104*, 9842.
- (23) Contescu, C.; Popa, V. T.; Schwarz, J. A. *J. Colloid Interface Sci.* **1996**, *180*, 149.
- (24) Dehnicke, K.; Straehle, J. *Angew. Chem.* **1981**, *93*, 451.
- (25) Zhuang, J.; Rusu, C. N.; Yates, J. T. *J. Phys. Chem. B* **1999**, *103*, 6957.
- (26) Liao, L. F.; Wu, W. C.; Chuang, C. C.; Lin, J. L. *J. Phys. Chem. B* **2001**, *105*, 5928.
- (27) Rusu, C. N.; Yates, J. T. *J. Phys. Chem. B* **2001**, *105*, 2596.
- (28) Diwald, O.; Thompson, T. L.; Zubkov, T.; Goralski, E. G.; Walck, S. D.; Yates, J. T. *J. Phys. Chem. B* **2004**, *108*, 6004.